frontiers | Frontiers in Marine Science

TYPE Original Research
PUBLISHED 14 October 2024
DOI 10.3389/fmars.2024.1483768

OPEN ACCESS

EDITED BY
Yifei Zhao,
Nanjing Normal University, China

REVIEWED BY
Jianfeng Su,
Tongji University, China
Zhibing Feng,
East China University of Technology, China

*CORRESPONDENCE
Shihao Liu
shliu@sklec.ecnu.edu.cn

RECEIVED 20 August 2024
ACCEPTED 25 September 2024
PUBLISHED 14 October 2024

CITATION
An S, Feng A, Feng W, Wang YP, Chen Y, Wu Z, Chen X, Yu Y, Pan Y and Liu S (2024) Development and distribution of submarine channels associated with sediment gravity flows in the modern Huanghe (Yellow River) subaqueous delta.
Front. Mar. Sci. 11:1483768.
doi: 10.3389/fmars.2024.1483768

Development and distribution of submarine channels associated with sediment gravity flows in the modern Huanghe (Yellow River) subaqueous delta

Shikang An[1], Aiping Feng[2], Wei Feng[1], Ya Ping Wang[1,3], Yufeng Chen[4], Zhuoyi Wu[1], Xiaolong Chen[1], Yonggui Yu[5], Yupeng Pan[3] and Shihao Liu[1]*

[1]State Key Laboratory of Estuarine and Coastal Research, East China Normal University, Shanghai, China, [2]Fourth Institute of Oceanography, Ministry of Natural Resources, Beihai, China, [3]Ministry of Education Key Laboratory for Coast and Island Development, School of Geographic and Oceanographic Sciences, Nanjing University, Nanjing, China, [4]Engineering Survey Branch, Huadong Engineering (Fujian) Corporation Limited, POWERCHINA Huadong Engineering Corporation Limited, Hangzhou, China, [5]First Institute of Oceanography, Ministry of Natural Resources, Qingdao, China

Background: Gravity-driven depositional processes play a pivotal role in shaping the geomorphology of subaqueous deltas worldwide, particularly by eroding the seafloor, leading to the formation of rugged submarine channels (SCs) and triggering various subaqueous geohazards. A comprehensive understanding of SCs is crucial for elucidating these depositional mechanisms and mitigating the risks associated with submarine geohazards. Although SCs in the Huanghe delta front have been previously identified, often described as seafloor gullies or subsurface "disturbed strata," most studies have primarily concentrated on their engineering geological properties. However, there has been limited research on the scale, morphology, and development of these SCs, especially those that are buried within the stratigraphy.

Methods: This study integrates high-resolution sub-bottom data, sediment core analyses, and historical bathymetric data to investigate the morphology, distribution, and formation mechanisms of SCs in the Huanghe subaqueous delta.

Results: The SCs, both buried and exposed, are widespread along the middle and upper delta front, predominantly located at or near the landward flank of sediment gravity flow (SGF) -related accumulations. The buried SCs are characterized by cut-and-fill structures with transparent to semi-transparent fills, indicating rapid infilling processes as SGF energy dissipates. These buried channels were preserved within different sets of delta front deposits formed during 1855–1964 CE, 1964–1976 CE, and 1976–2007 CE, with the latter two periods separated by a significant lobe-switching event in 1976 CE. This event, combined with prevailing southeastward sediment transport and erosional regimes, appears to have controlled the preservation of SCs along the delta front: SCs in the Diaokou Lobe's delta front (pre-1976) suffered significant erosion, leaving only one set of channel (erosional remnants) preserved, while the SCs in the Qingshuigou Lobe's delta front (post-1976) are characterized by

well-preserved, multi-phase channels at different horizons. The cross-section morphology of the SCs reveal three primary types: symmetrical, asymmetrical, and composite, corresponding respectively to (1) idealized SGF incision, (2) uneven incision intensity on either side of the SCs, and (3) the merging of two or more symmetrical/asymmetrical SCs.

Conclusions: We describe in detail the morphology, distribution and development of SCs in the modern Huanghe subaqueous delta. These findings provide insights into the formation and distribution of SCs in other shallow marine settings, particularly in delta front areas, and potentially offer information for disaster prevention and engineering development in such regions.

KEYWORDS

delta front, sediment gravity flow, submarine channel, Huanghe delta, seismic profile

1 Introduction

The high-density sediment gravity flow (SGF) possesses a scouring force when it is transported downslope due to carrying a large amount of sediments (Mulder et al., 2003). When the energy of SGFs exceeds the critical threshold for eroding the underlying sediments, they erode the under-consolidated sediments below to increase their sediment concentration and maintain continuous downslope momentum, thereby forming submarine channels (SCs) (Prior et al., 1986; Xu, 2014; Luan et al., 2018). SCs are key geomorphological features for identifying SGF events and the basis for further refining regional sedimentation analysis. They have been frequently reported in continental slopes, lake basins, and submarine canyons (Daly, 1936; Malonely et al., 2020; Tang, 2020), with generally large scales and relatively fixed paths. Because of the gentle slope in shallow-water environments, the resulting "SCs" are small in size, short in length, and vary in temporal and spatial location. They are therefore initially referred to as "gullies", "seafloor depressions", or " cut-and-fill structures", and these terms have been used extensively in subsequent studies (Coleman et al., 1980; Jeng, 2001; Vanneste et al., 2014; Roberts et al., 2020; Wang et al., 2020). Due to frequent river avulsions and ongoing delta degradation, deposition in subaqueous delta has becoming more and more unstable (Yang et al., 2017; Prasojo et al., 2024). This increases the possibility of SCs forming, further complicating the depositional environment. Nevertheless, the extent and formation mechanisms of SCs in subaqueous delta front in the context of lobe switching remains unclear.

The modern Huanghe Delta (MHD, the latest present-day active superlobe) has experienced frequent and long-lived SGF events, including hyperpycnal flows and collapse/resuspension-related turbidity flows (Wright et al., 1986; Masson et al., 2006). Additionally, frequent avulsions of the Huanghe and mutual overlap of the delta lobes cause frequent and extensive SGFs within the study area (Figure 1C), leading to the formation of numerous SCs (Liu et al., 2022). The longshore transport and/or erosional regimes/ longshore drift (tidal actions, waves, residual currents, and their combination) offshore of MHD further increase the difficulty in identifying SCs and analyzing their sedimentary evolution.

The rapid sedimentation and under-consolidated nature make the Huanghe subaqueous delta create one of the most challenging marine engineering environments. In this context, some studies have referred to the "SCs" on the Huanghe subaqueous delta seafloor as subsurface "disturbed strata" or "weak layers" (Chen and Yang, 1992; Xu et al., 2008; Li, 2015) and have analyzed them as part of the geological system, focusing on their 3D morphology, formation and development mechanisms (Yang et al., 1994; Peng et al., 2014; Malonely et al., 2020). However, most of this research has primarily addressed exposed or partially buried SCs (e.g., Peng et al., 2014; Wang et al., 2020), with a particular emphasis on their engineering geological properties.

Many studies have identified SCs, exhibited as cut-and-fill structures, buried within the subsurface stratigraphy of the Huanghe subaqueous delta (Prior et al., 1986; Chen and Yang, 1992; Liu et al., 2022). However, their morphology, distribution, and formation mechanisms remain less explored, largely due to the lack of dense, high-resolution seismic data. These SCs can incise several meters into different seismic units (Liu et al., 2022), further complicating the stratigraphy of the subaqueous delta. In this regard, beyond their importance in engineering geology, the study of buried SCs is also essential for understanding the sub-decadal to decadal-scale sedimentary evolution of the modern Huanghe subaqueous delta front.

In this study, we aim to conduct a detailed analysis of SCs, with a particular focus on the previously under-studied buried SCs, utilizing dense high-resolution sub-bottom data, along with reexamining previously published historical bathymetric and borehole data, from the delta front near and between the Diaokou Lobe (DKL) and Qingshuigou Lobe (QSGL) of the MHD (Figure 1).

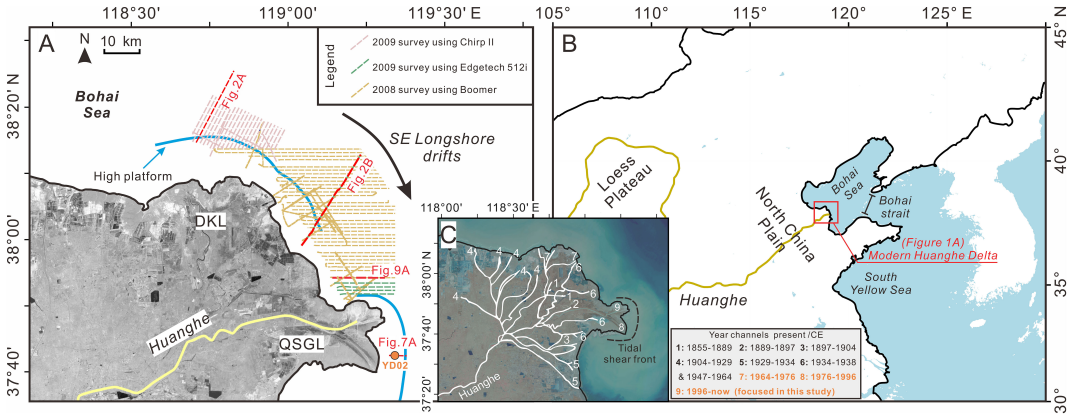

FIGURE 1
(A) Map of the modern Huanghe Delta (MHD) showing the locations of seismic survey track and core YD02. The blue solid lines indicate the seaward boundary of high platform, while the black arrow indicates the direction of longshore drift. **(B)** Location map of the MHD. **(C)** A 2008 CE satellite image detailing the physiography of MHD and the tidal shear front (black dotted line; after Li et al., 1994), overlaid with the historical channels on the MHD (white lines; after Xue, 1994).

The primary objectives are to explore: (1) the correlation between SCs and previously documented sediment gravity flows (SGFs); (2) the morphology and spatial distribution of SCs in the Huanghe subaqueous delta; and (3) the evolution of SCs under the influence of the prevailing sediment transport regime and the lobe-switching event in the MHD.

2 The study area

2.1 Environmental setting

The Huanghe originates from the Qinghai-Tibet Plateau, passes through the Loess Plateau and North China Plain before emptying into the Bohai Sea (Figure 1B), with a total length of 5460 km (Xue, 1993; Yu et al., 2013). The high sediment discharge (an average annual sediment discharge of 6.88×10^8 t) of the Huanghe has caused frequent avulsions, leading to continuous shifts in its lower reaches over the past 6000 years, forming 10 deltaic superlobes (Bi et al., 2021). Except one located in the Yellow Sea (1128–1855 CE), all of the superlobes are located in the Bohai Sea, a semi-enclosed marginal sea located off the northeast coast of China with an average water depth of ca. 18 m.

After avulsion at Tongwaxiang, the Huanghe shifted northward into the Bohai Sea, and the MHD began to prograde in 1855 CE, covering an area of ca. 6000 km^2 (Pang and Si, 1980; Wang and Ye 1990; Yu et al., 2013) (Figures 1A, B). Eight delta lobes of the latest present-day active superlobe (the MHD) have formed along the southwestern coast of the Bohai Sea due to frequent avulsions and lobe-switching events (Pang, 1979; Xue, 1994, 2009; Liu et al., 2019) (Figure 1C). Among these, the DKL was activated from 1964 to 1976 CE (Figures 1A, C); while active accumulation of the QSGL (the present-day active delta lobe) and abandonment/degradation of the DKL were as a result of the latest major avulsion of Huanghe at southeast of DKL in 1976 CE (Chu et al., 2006) (Figures 1A, C).

2.2 Climatic and hydrodynamic conditions

The MHD is located in a temperate monsoon region. Under the control of the East Asian monsoon, the wave direction shifts with the wind direction, primarily southeast in the summer and northeast (strong waves of over 3 m wave height) in the winter (Luo and Liu, 2015; Ren et al., 2022). In addition, the water and sediment discharge of the Huanghe also exhibit pronounced seasonal variations, with the average water and sediment discharge during the flood season (July to November) accounting for 80% of the annual total (Cheng and Cheng, 2000; Fan et al., 2006; Yang et al., 2008).

The coastal zone off the Huanghe mouth is micro-tidal with semidiurnal tidal patterns (Xiong, 2012). The tidal range is small, averaging between 0.22 m and 1.0 m, with velocities of 0.5–1.0 m/s (Zhao et al., 1995; Ye et al., 2023). The southeast flood tidal currents are stronger (velocity up to 2.2 m/s) than the northwest ebb tidal currents (Zhang et al., 1998; Fan et al., 2006). After filtering out tidal and other periodic currents, residual currents persist (Bi et al., 2014), from northwest to southeast, with velocities between 0.1–0.3 m/s, and is the main driving force for sediment transport in the Huanghe (Liu, 1985; Wang, 1989; Wang et al., 2014). Tides, waves, and residual currents together form the longshore transport and/or erosional regimes along the southwest coast of the Bohai Sea (Chen, 2009; Fu et al., 2021) (Figure 1A).

There is also a tidal shear front roughly parallel to the coastline near the present-day active river mouth (east of the QSGL) (Figure 1C), characterized by low flow velocities and converging flow directions on either side (Wang et al., 2024). Due to the significant differences in hydrodynamic characteristics between the frontal zones (Bi et al., 2011), a substantial amount of sediment (ca. 50%) is trapped by the tidal shear front, with most sediments depositing within 15 m of water depth (Li et al., 2001; Wang et al., 2007). This leads to the formation of a "high platform" (ca. 15 m thick) in the upstream region of the delta front (Figure 1A), connected to the steep delta front slope at its seaward end (the

middle and lower parts of the delta front), creating geomorphological conditions conducive to the formation of sediments gravity flows (Liu et al., 2022).

2.3 Brief retrospective of SC studies in the MHD

To our knowledge, the earliest documentation of cut-and-fill structures, described as moderately disturbed areas just below the seafloor near the QSGL, was provided by Prior et al. (1986) using high-resolution geophysical surveys. Liu et al. (2022) identified both buried and active (exposed on the seafloor) SCs that are widespread off the and the regions between the DKL and QSGL. These features have been attributed to hyperpycnal flows, mass movements, and resuspension-related SGFs. Other studies have also linked the formation of these disturbed areas to processes such as liquefaction, submarine landslides, scouring, and deformation sliding (Xu et al., 2009; Li, 2015; Wang et al., 2020; Yu et al., 2022).

From a geotechnical perspective, SCs are widely recognized as an unfavorable geological condition and a significant concern (Peng et al., 2014). They are considered potential triggers for various subaqueous geohazards, such as submarine slumps, regional landslides, and differential erosion, posing serious threats to marine engineering facilities (Gao, 2011). As a result, regions with SCs are generally avoided when selecting sites for marine engineering structures (Xu et al., 2008; Wen et al., 2018). However, comprehensive analyses of SCs (whether buried or exposed) across the entire Huanghe subaqueous delta front are still limited. Most studies have focused on relatively small areas and lacked high-resolution geophysical data covering a wide extent of the delta front, which has resulted in a gap in understanding the distribution and evolution of SCs in relation to the overall development of the MHD.

3 Materials and methods

3.1 Seismic data acquisition and processing

The high-resolution seismic data used in this study were obtained from three seismic surveys conducted between 2008 and 2009 CE in the subaqueous areas of the MHD (Figure 1A). In 2008 CE, the boomer data were collected using a CSP2200 sub-bottom profiling system (Applied Acoustic Engineering Co., UK) with a source power of 300–500 J; in 2009, the chirp data (first reported) were collected using a Geoacoustics Chirp II system (GeoAcoustics Ltd., UK) with a source frequency range of 2–7 kHz and an Edgetech 3100P system equipped with a 512i towfish (Edgetech Co., USA) with a source frequency range of 0.7–12 kHz. In total, approximately 1500 km of seismic profiles were obtained. The seismic survey tracks covered the southwestern part of the Bohai Sea, with water depths ranging from 5 to 25 m, covering multiple subaqueous delta lobes (Figures 1B, C). The Boomer data and Edgetech chirp seismic data used in this study have been partly reported (Liu et al., 2014, 2016, 2022). Focusing on the formation mechanism of SCs, this study further interprets these data in combination with additional data.

All seismic data were processed using Madagascar 2.0 software (http://www.ahay.org/wiki/Main_Page), including swell filtering, automatic gain control, and water column muting. Subsequently, the processed seismic data were interpreted using DecisionSpace™ software (Halliburton Co, US), including the identification and tracking of stratigraphic surfaces and seismic units, and the recognition of SGF-related accumulations and SCs based on the configuration of the reflection and superposition. Following previous studies, the two-way travel time (TWTT) was converted to depth using an average acoustic velocity of 1650 m/s (Liu et al., 2014, 2016).

3.2 Borehole data

To understand the lithology characteristics of the SCs, a published core (YD02, 119.35°E, 37.71°N) collected offshore of the QSGL in 2018 CE (Chen et al., 2021) was reviewed in this study. Part of the data was reprocessed for analysis with special emphasis on the lithology of SCs, including raw grain size data (sampled at 3 cm intervals) and core photographs.

4 Results

4.1 Seismic stratigraphy

Our seismic stratigraphy interpretation, particularly the identification of SGF-related seismic units, is consistent with Liu et al. (2022), with a primary focus on the SCs. We identified a pronounced, sub-horizontal unconformity (the MHD base) at depths 15–25 m below the sea level. This unconformity was formed under a dominant erosional regime after the Huanghe River's rechanneling to discharge into the southern Yellow Sea between 1128 and 1855 CE (Liu et al., 2016, 2022). The sediments overlaying this surface correspond to the MHD and are divided into units A, B, and C (Figure 2). Unit C, the lowest, features internal reflections that converge seaward, forming a representative Gilbert-type clinoform (Figure 2), corresponding to the older MHD clinoform described by Liu et al. (2022). Together, Units B and C form an apron-like (or wedge-like) accumulation body superimposed on the bottomset of the older MHD clinoform, with their internal reflections downlapping onto the MHD base. These two units correspond to the previously mentioned SGF-related accumulations, with their boundary surface, R2, formed in association with the lobe-switching event in 1976 CE (Figure 2). As with Liu et al. (2022), SCs are characterized by both cut-and-fill structures buried within units A, B, and C, and gullied/jagged seafloor features (Figure 2). The reflective characteristics, morphology, and spatial distribution of these SCs, which are the focus of this study, are described in detail later.

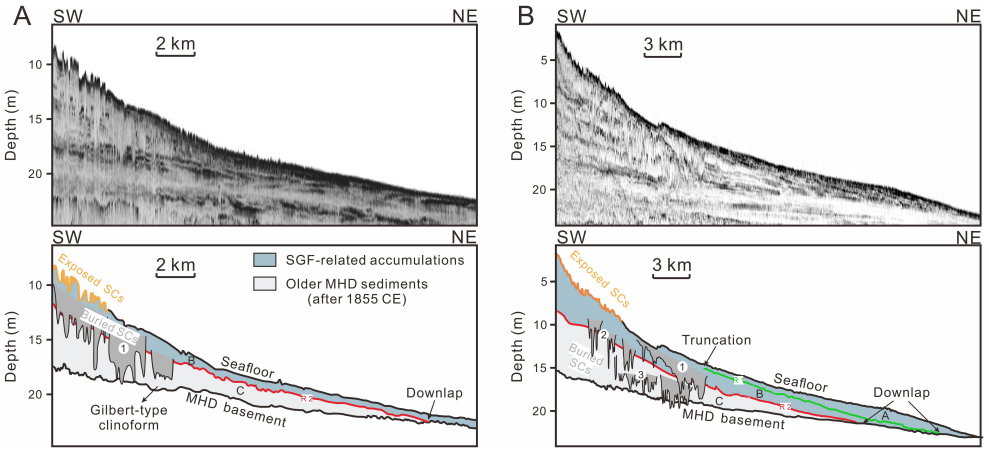

FIGURE 2
Uninterpreted (top) and interpreted (bottom) shore-normal seismic profiles off the Diaokou Lobe (DKL) **(A)** and the Qingshuigou Lobe (QSGL) **(B)** modified after Liu et al., 2022). See Figure 1A for their locations. The submarine channels (SCs) are observable inside unit A, unit B and, unit C.

4.2 Sectional morphology of SCs

The seismic lines are oblique with the SCs in most cases (Figure 3), and to make the profiles provided in this study resemble along strike or dip direction of the SCs for further discussion, some representative profiles from the dense seismic data were selected to present (Figures 1, 3). Based on observation of numerous sub-bottom profiles, most SCs are rugged, and have jagged basement, with deeper incisions in the center, as depicted in Figures 4, 5, 6. The longitudinal axes of the SCs appear to be shore-normal given the widths of the SCs are generally greater in the profiles in shore-normal direction than in the that in shore-parallel direction (Figures 4–6). These SCs vary considerably in size, with widths ranging from 200 m to 6 km, and depths from 1 to 12 m below the sea level, and extend up to ca. 15 km in the shore-normal direction (Figures 4–6). Based on whether or not buried, SCs are divided into two main types:

Exposed/active SCs (jagged/gullied seafloor): Such SCs appear as jagged/gullied seafloor, distinguished from flat surfaces, and are not filled or not fully filled with sediments (Figure 4). They are present in both the abandoned DKL and the active QSGL, with more occur near the DKL.

Buried SCs (subsurface cut-and-fill structures): These SCs are observed in both the abandoned DKL and the active QSGL (Figure 4). They are buried below the seafloor in seismic units A, B, and C, and incising several meters (exceed ca. 10 m) into the underlying seismic units (Figure 4). The parallel/sub-parallel reflections within the units A, B, and C are truncated by such buried SCs (Figure 4). Two types of acoustic reflections of the filling deposits of buried SCs are observed, e.g., acoustically transparent and chaotic reflection (Figure 5). The acoustically transparent fills lack clear stratification and discernible structures, indicating a homogeneous and structureless character, while acoustically chaotic fills suggest heterogeneous and poorly sorted fill

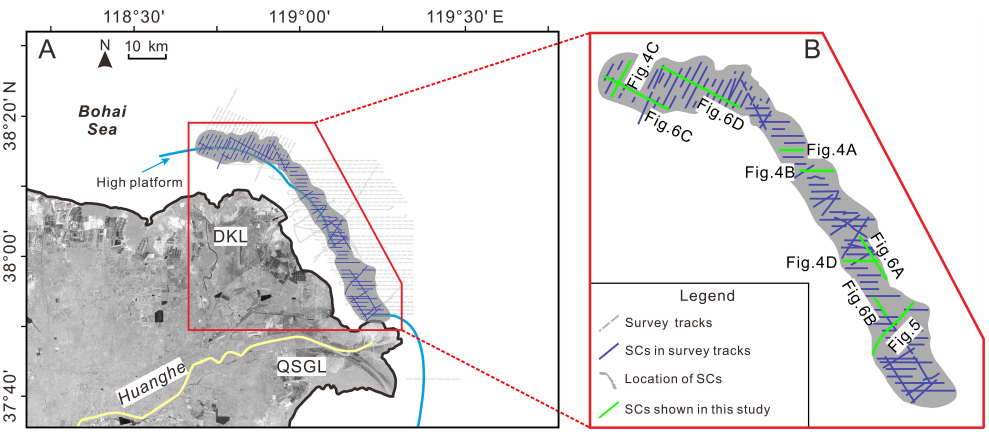

FIGURE 3
(A) Distribution of SCs and their relationship with high platform. **(B)** An enlarged view of the distribution map. The deep blue lines indicate the locations of the SCs identified in corresponding seismic profiles.

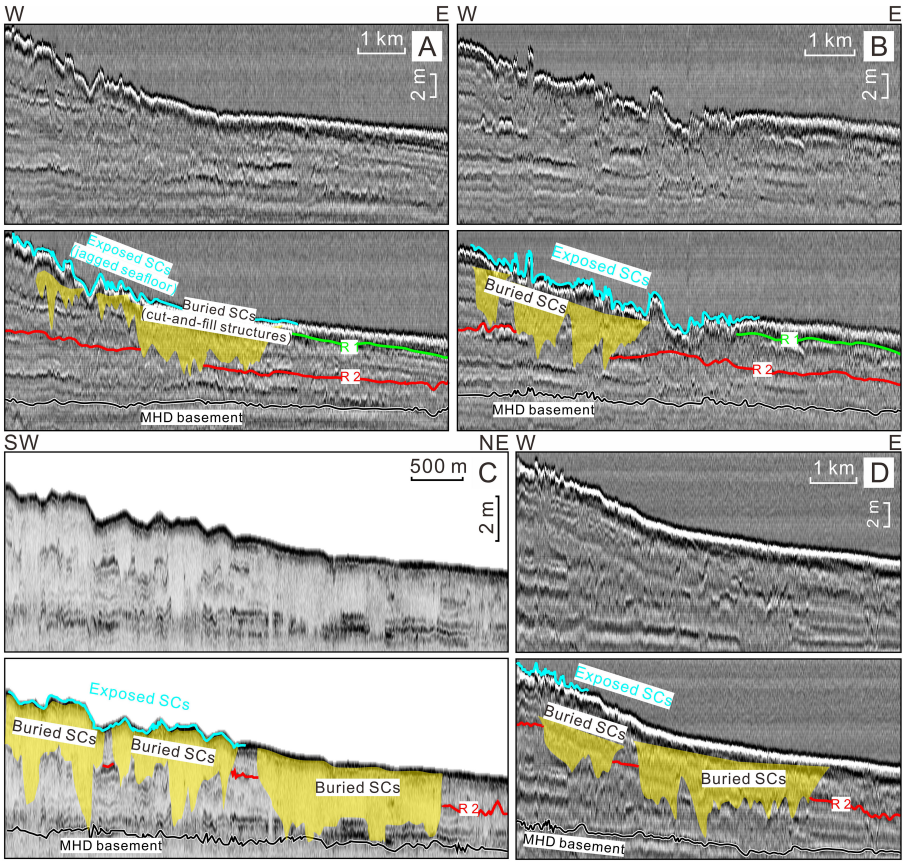

FIGURE 4
(A–D) Uninterpreted (top) and interpreted (bottom) shore-normal seismic profiles showing the characteristics of buried SCs (cut-and-fill structures) and exposed SCs (jagged/gullied seafloor). See Figure 3B for their locations.

sediments (Liu et al., 2013) (Figure 5). Notably, the relief of exposed SCs is lower compared with the jagged basement of buried SCs (Figure 4).

Buried SCs exhibit varying cross-sectional characteristics in the shore-parallel direction, which can be categorized into three types: symmetrical, asymmetrical, and composite SCs (Figure 6).

Symmetrical SCs: Such SCs typically display a U-shaped or V-shaped cross-sectional shape with nearly same slope gradients on both sides (Figure 6). This kind of SCs is less frequently observed and smaller in size, with the maximum width not exceeding 1 km (Figure 6).

Asymmetrical SCs: These SCs feature uneven slopes on both sides, with a tilted surface or irregular depressions at the bottom (Figure 6). Their sizes are comparable to that of the symmetric SCs, with widths up to 1 km and a maximum depth of ca. 6 m below the sea level (Figure 6). Asymmetrical types are less frequently observed among the identified SCs (Figure 6).

Composite SCs: These SCs are primarily the merging of two or more of the previously described types (symmetrical and asymmetrical SCs) of SCs (Figure 6), which account for a large proportion of the observed SCs. They are larger in scale, with a maximum width of ca. 8 km and a maximum depth of ca. 6 m (Figure 6).

4.3 Spatial distribution of SCs

Following a detailed analysis of high-resolution seismic profiles, numerous SCs have been identified (Figure 3). These SCs are generally distributed at/near the landward flank of the SGF-related accumulations (upper delta front) and along the delta front slope, which lies between the high platform and the toe of the delta front, up to ca. 10 km away from the shore (Figures 2, 3).

The SCs distributed area exhibit an elongated, shore-parallel shape, spanning almost the entire subaqueous delta of the DKL and the northern subaqueous delta of the QSGL (Figure 3A). It has a length of ca. 70 km in the shore-parallel direction and a width of 2–10 km in the shore-normal direction (Figure 3A). The whole range of the SCs distribution in the Huanghe subaqueous delta remains not fully uncovered due to the limited coverage of the existing seismic data. Nevertheless, based on the identified spatial distribution of SCs, it is reasonable to infer that their distribution may extend beyond the seismic data coverage area, potentially including the western part of DKL and the eastern part of QSGL (the eastern part of the present-day active river mouth).

In cross-sections perpendicular to the shoreline, exposed SCs are distributed throughout the study area. Buried SCs are more

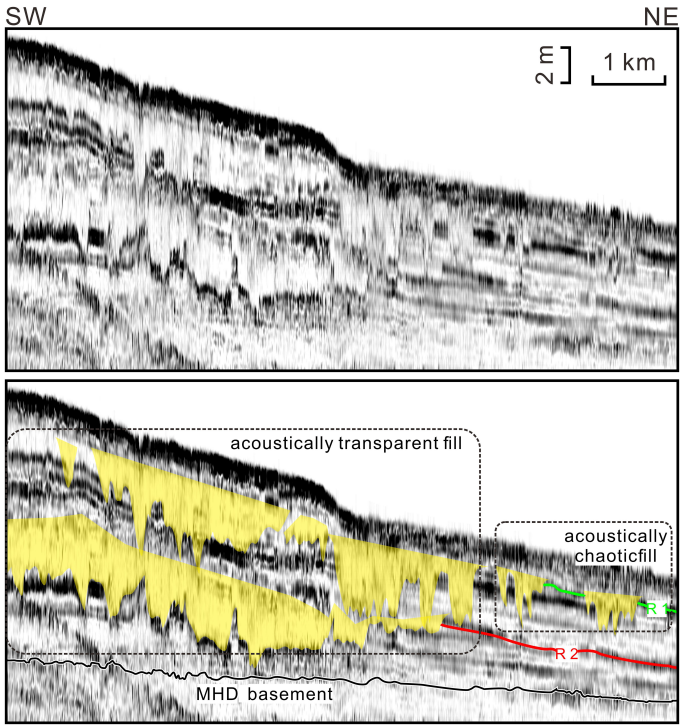

FIGURE 5
Enlarged shore-normal seismic profiles, presented both uninterpreted (top) and interpreted (bottom), detailing the acoustic characteristics of the fill within buried SCs, which include both transparent material and chaotic reflections. See Figure 3B for its location.

concentrated, forming clusters, with most located at depths between 5 and 25 m below the sea level (Figures 4–6). From the DKL to the QSGL, buried SCs display varying burial depth characteristics. Seismic profiles near the DKL area show that SCs are embedded into nearly the same depth below the seafloor, within unit A (SC1 in Figure 2A). In contrast, SCs near the QSGL area are embedded below the seafloor into several distinct depths, concentrated within units A, B, and C (SC1, 2, and 3 in Figure 2B).

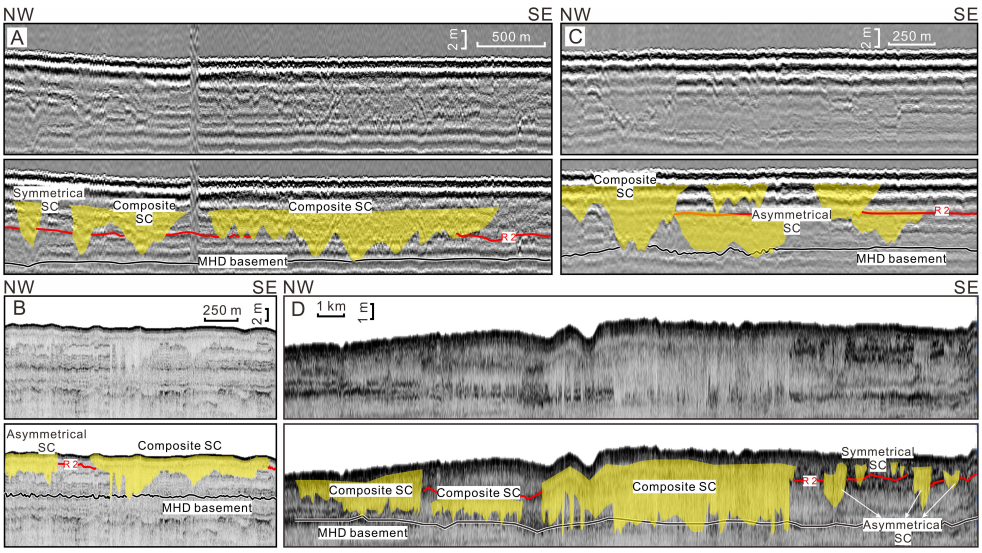

FIGURE 6
(A–D) Enlarged shore-parallel seismic profiles, presented both uninterpreted (top) and interpreted (bottom), illustrating the identification of symmetrical, asymmetric, and composite SCs. See Figure 3B for their locations.

4.4 Lithology of core YD02

Core YD02, which penetrated the buried SCs (Figure 7), provides a valuable opportunity for analyzing the sedimentary characteristics of the fill of the buried SCs.

Poorly sorted, gray-brown silt/fine sand and interlayered organic material characterize the interval of 0.3–2 m in core YD02, producing an upward-fining succession, with sand layers in the uppermost 0.2 m and wavy thin clay/silt bedding in 0.80–0.85 m (Figure 7B). Between 2 and 4 m is mostly made up of yellow-brown silt and bioturbation, with many interbedded sand/mud layers. The lower section (4.0–9.23 m) is a comparatively homogeneous, structureless layer of yellow-brown/gray-brown silt (Figure 7B). The blue-gray fine sand in this core is between 9.23 and 10 m (Figure 7B).

5 Discussion

5.1 Interpretation of core lithology

The correlation between the seismic stratigraphy and the core YD02 is illustrated in Figure 7A. The core was retrieved 9 years later that the acquisition of the seismic profile in 2009 CE, during which a significant difference in water depth is produced due to sediment accumulation. Therefore, there is a certain discrepancy between the seafloor and the top of the core YD02 (Figure 7A).

The most prominent correlation is at depths of 6.2–6.5 m and 9.10–9.24 m (homogeneous, structureless gray-brown silt) in core YD02, which corresponds to the internal of buried SCs (Figure 7). This composition is consistent with the lithological characteristics observed in numerous SCs worldwide (e.g., Mulder et al., 2003; Correggiar et al., 2005a). The interval of poorly sorted, gray-brown silt/fine sand from 0.3 to 2 m, which is consistent with the lithology of many SGF-dominated sediments at the toes of the delta front (Mulder and Alexander, 2001), suggests that they were deposited by SGFs (Figure 7B). The 0.3-2 m section is missing from the seismic data, suggesting that it was deposited between 2008 and 2018 CE. The observed upward-fining trend could potentially be linked to the annual water and sediment regulation scheme implemented since 2002 CE (Chen et al., 2021). During the early stages of water and sediment regulation scheme, the downstream riverbed underwent significant erosion, causing the grain size entering the sea to become coarser. However, as the riverbed's resistance to erosion strengthened over time, the supply of coarse-grained sediments from the downstream area diminished, leading to a finer sediment deposition into the sea (Wu et al., 2017; Jiang et al., 2018). Additionally, the core YD02 contains a significant amount of conventional deltaic mud accumulations (e.g.,

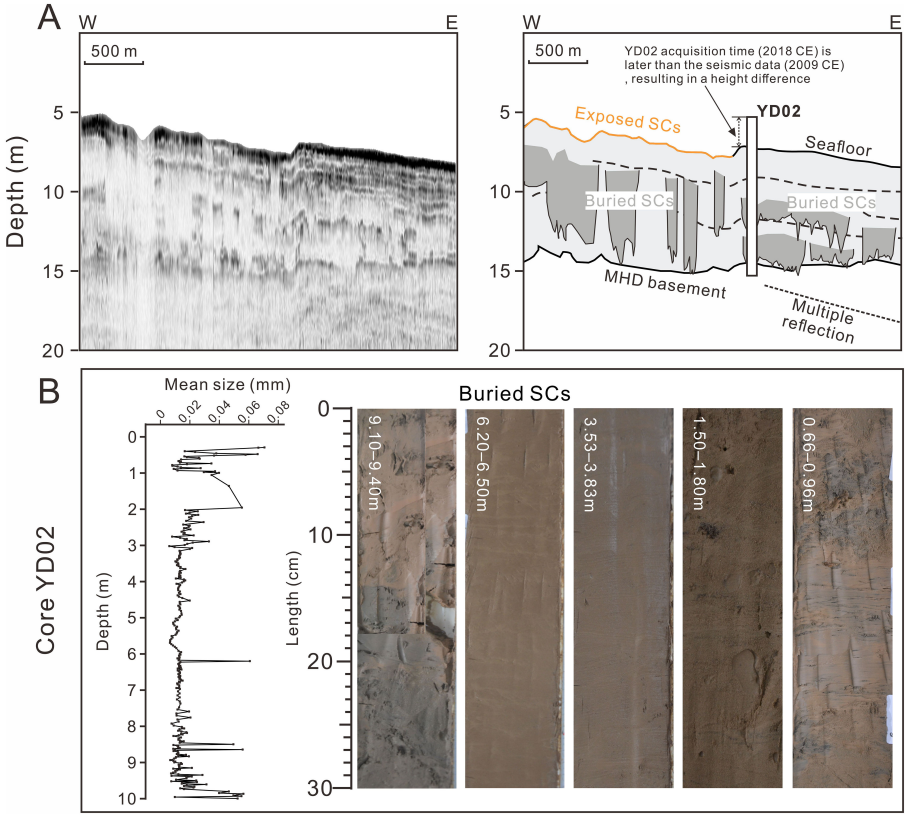

FIGURE 7
(A) Shore-normal seismic profile, shown both uninterpreted (left) and interpreted (right), intersecting core YD02, illustrating the correlation between seismic stratigraphy and core. See Figure 1A for their locations. **(B)** Mean grain size and representative photographs of SC fills from core YD02 (modified after Chen et al., 2021).

Zhou et al., 2016; Hu et al., 2024), and lithology characteristics indicative of the longshore transport and/or erosional regimes reworking (Fan et al., 2013; Chen et al., 2021) (Figure 7B), e.g., interbedded sand/mud layers and bioturbation.

5.2 SGFs as key drivers of SC formation in the delta front

We utilizing more extensive and denser seismic data, conclude that the buried SCs found in the Huanghe subaqueous delta are formed by the incision of the seafloor during the downslope transport of SGFs, eventually rapid deposit on the upper delta front/downlapping SGF-related accumulations (Figure 2). Our findings are compared with previous hypotheses that attributed buried SCs (cut-and-fill structures) to submarine geohazards such as sediment liquefaction, slumping, and submarine landslides (e.g., Feng et al., 2004; Wang and Liu, 2016). This section focuses on discussing the seismic data evidence supporting this conclusion:

(1) According to previous studies, the origin of "cut-and-fill structures" is often associated with the collapse depression feature formed after hydrodynamic disturbances, where sediments gradually move downslope and spill over the initial arched failure area; Finally, erosive silt flow tongues slide downslope, forming cut-and-fill structures (Wang et al., 2020). Our seismic data indicate that the buried SCs basement is irregularly jagged (Figure 4), which contrasts with the smooth basement created by slides (Yu et al., 2022). The preserved steep incision of the SCs basement suggests that the internal sediments were rapidly infilled after the incision (Correggiar et al., 2005b) (Figure 8C). Based on this, we propose that the buried SCs observed in the MHD are more likely formed by erosion.

(2) The SCs are generally located at/near the upper delta front/the landward flank of the SGF-related accumulations (seismic units A and B) (Figure 2), which is consistent with the position where SGF incise the seafloor (e.g., Zavala et al., 2011). The longitudinal axes of the SCs also appear to be consistent with the direction of downslope transport of the SGF sediment (e.g., Liu et al., 2022) (Figures 4–6). Both features indicate a strong correlation between SCs and SGFs.

(3) The SCs driven by SGFs can also explain why the relief at the exposed SCs' basement is generally smaller than that of buried SCs (Figure 4). A possible explanation is that SCs may still be filled with sediments after the seafloor is incised by SGFs, ultimately reducing the reliefs. Alternatively, the erosive intensity of the SGFs forming exposed SCs may has decreased compared to earlier periods. Since the lobe switched to the QSGL in 1976 CE, collapse-related turbidity flows have frequently occurred in the study area, transporting large masses from the upper delta front to the middle and lower delta front, thereby significantly reducing the delta front slope (Prior et al., 1986; Bi et al., 2021; Liu et al., 2022) (Figure 9B), which in turn has reduced the frequency and erosive intensity of these flows. This will be discussed in detail in subsequent sections.

(4) The cut-and-fill characteristics of buried SCs are consistent with buried SCs driven by SGFs in several delta fronts worldwide, including the Yangtze Delta (Feng et al., 2024), the Mississippi Delta (Malonely et al., 2020), the modern Po Delta (Correggiar et al., 2005b), and many other ancient and modern deltas (Dasgupta and Buatois, 2015). Numerous lithological characteristics of cores in previous studies also indicate that the interiors of SCs in the Huanghe subaqueous delta are predominantly composed of homogeneous (acoustically transparent material), high water content clay or silt (e.g., Liu et al., 2014; Zhou et al., 2016) (Figure 7B), which is inconsistent with the loose, lower water content sediment characteristics following liquefaction and slumping in previous studies (e.g., Chang and Jia, 2010).

Based on the above evidence and previous studies (Zavala et al., 2006; Xu, 2014), this paper further explained the complete evolution process of the cut-and-fill structures of SCs (Figure 8): Initially, SGFs are generated at the upper slope of the subaqueous delta, with their flow velocity increasing continuously as they move downslope (Figure 8A). When the velocity exceeds the erosion threshold, SGFs will incise the seafloor, forming gullied SCs (Figure 8B). As these flows continue downslope, they persist in their erosive action, causing the SCs to enlarge along the slope (Figure 8B). Eventually, the SGFs attenuate in a pulsating manner, and the sediments they carry gradually deposit, ultimately forming the cut-fill structures of SCs (Xu, 2014) (Figure 8C).

5.3 Development of diverse sectional morphology and features of SCs

5.3.1 Timing of SC formation

Although the bathymetric data and seismic data were not collected in the same year, the corresponding bathymetric profiles generally overlap with the main stratigraphic unit boundaries within the MHD. Therefore, historical bathymetric data can provide approximate age constraints for the SCs in the study area (e.g., Xue et al., 2009; Yu et al., 2013; Liu et al., 2022) (Figure 9). We found that the SCs were roughly formed in three time periods: (1) during the active QSGL period in 1976–2007 CE (SC1 in Figure 9A); (2) during the active DKL period in 1964–1976 CE (SC2 in Figure 9A); and (3) during the formation period of the MHD in 1855–1964 CE (SC3 in Figure 9A). The SGF-related accumulations at the toe of the delta front have incorporated the conventional deltaic accumulations (i.e., the aforementioned Gilbert-type clinoform of the delta front) from 1855 to 1964 CE, so there is no clear seismic horizon of the SGF-related accumulations, but the existence of numerous SCs can still prove the frequent occurrence of SGFs. The evolution of the two SGF-related accumulations (units A and B) is coeval with the downslope sediment-transport regimes of the SCs, which are the focus of subsequent discussion (Figures 2, 9).

From 1968 to 1976 CE, during the active accumulation period of the DKL, hyperpycnal flows frequently originated from the delta front slope (Wright et al., 1986) and were the primary mechanism for sediment deposition at the delta front (Wrihjt et al., 1988), as evidenced by the net accumulation (Figure 9A). Consequently, from 1964 to 1976 CE, the SGFs in the study area were predominantly driven by hyperpycnal flows. The river channel shifted eastward to its present course in 1976 CE (Figure 1C), enabling the active

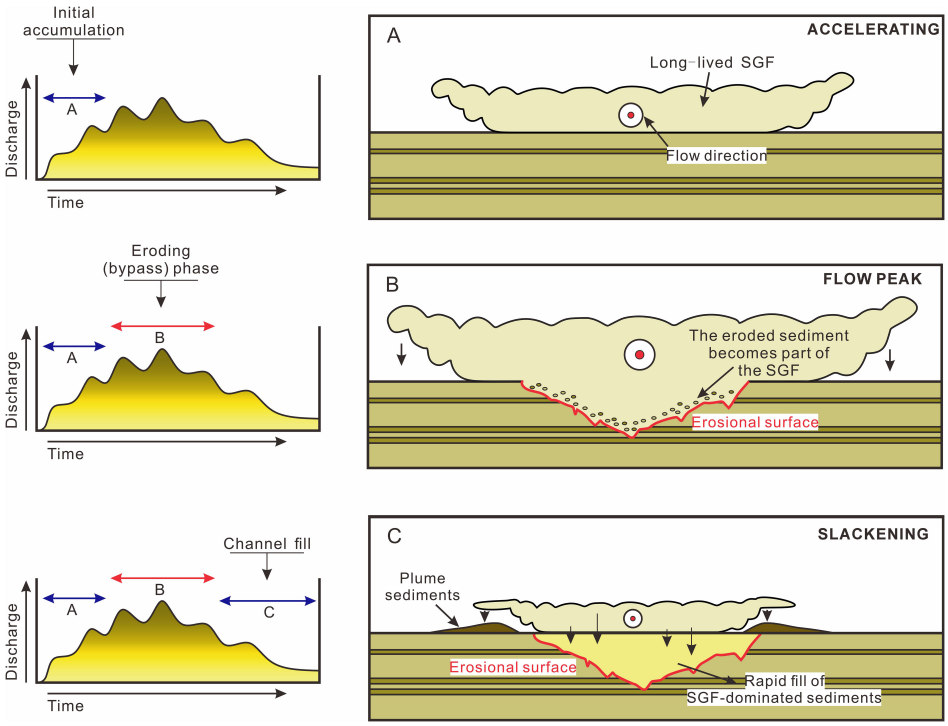

FIGURE 8
Schematic diagram detailing the sedimentary processes and evolution of SGF-driven cut-and-fill structures (modified after Zavala et al., 2006), which can be divided into Initial accumulation phase **(A)**, Eroding phase **(B)**, and Channel fill phase **(C)**.

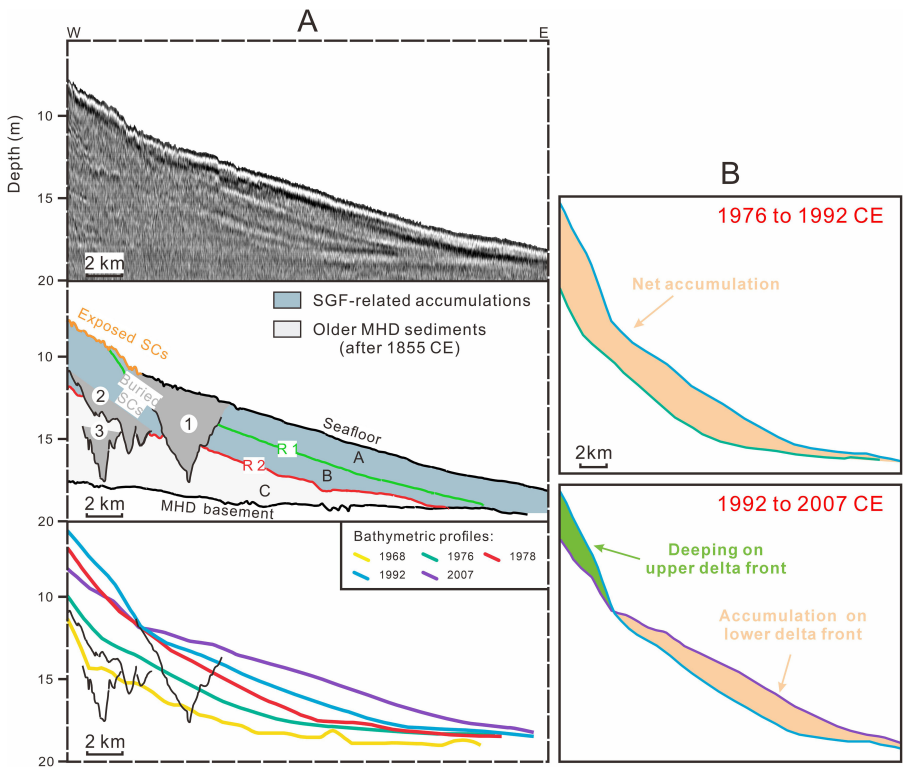

FIGURE 9
(A) SCs depicted in a representative seismic profile (see Figure 1A for its location), overlain with historical bathymetric profiles to provide approximate age constraints for the SCs. **(B)** Depth change maps in different years according to historical bathymetric changes (modified after Liu et al., 2022).

accumulation of the QSGL. From then on, the hyperpycnal flows formed at the river mouth were difficult to reach the northwest (opposite to the direction of the longshore drift). However, due to the enrichment effect of the Huanghe tidal shear front on suspended sediments near QSGL, substantial amounts of under-consolidated sediments accumulated on the high platform between the DKL and QSGL, which result in collapses frequently (Li et al., 2000; Masson et al., 2006) (Figures 1B, C). As previously mentioned, the SGFs in the area were predominantly driven by failure/collapse/resuspension-related turbidity flows after 1976 CE, as further evidenced by in bathymetric changes (deepening of the upper delta front and accumulation of the middle delta front) (Liu et al., 2022) (Figure 9B).

In summary, the deeply buried SCs formed before 1976 CE (Figures 2, 9) primarily resulted from the erosive action of hyperpycnal flows, whereas those formed after 1976 CE (more shallowly buried and exposed SCs) resulted mainly from failure/collapse/resuspension-related turbidity flows (Liu et al., 2022) (Figures 2, 9). The exposed/active SCs on the seafloor suggest that they have formed recently or are forming, yet to be filled and covered by subsequent sediments (Figure 4). Due to the frequent SGFs (hyperpycnal flows and turbidity flows) on the MHD (rather than single-event occurrences) (Wright et al., 1986; Wrihjt et al., 1988), multiple periods of buried SCs may have been formed by multiple SGF events over a short time span (Figures 2–9). Cross-sections of SCs in the shore-normal direction often show shallow incisions and minor jaggedness at both ends, with deeper incisions and more pronounced jaggedness in the middle (Figures 4–6), indicating that the incised intensity of hyperpycnal flows first increases and then decreases during downslope transport.

5.3.2 Origin of filling reflections in SCs

The acoustically transparent reflections in SCs mainly appeared in the middle and upper delta front (Figure 5). Core YD02 penetrated two sections of the SC, both characterized by acoustically transparent fill, as recorded in sub-bottom profiles (Figure 7B at depths of 6.2–6.5 m and 9.10–9.24 m). Structureless, higher water content silt makes up the interior of the acoustically transparent reflections of the SCs (Figure 7B), which are distinct from those found in core YD02 at other depths (Figure 7). Additionally, the mean grain size of buried SCs in core YD02 indicates a more quite uniform deposit of the SCs (Figure 7B). As we previously mentioned, the gullied/jagged basements of SCs result from the incision by SGFs (Zavala and Pan, 2018) (Figures 4–6). As SGFs transport downslope, the homogeneous fine-grained sediments are deposited more slowly at the tail of the flows or resuspended and redeposited (Zavala, 2020). The acoustically transparent reflections represent that the internal fill of buried SCs does not prevent the penetration of the acoustic signal and therefore represents the homogeneous sediments formed by slow deposition at the tail of the SGFs (Feng et al., 2024) (Figure 5), which are consistent with lithology features of core YD02 (Figure 7B).

Conversely, when SGFs transport downslope, their coarse-grained sediments, heavier and prone to further transport (as the main body of SGFs, it has more energy), deposit quickly with poor sorting (Lamb and Mohrig, 2009), resulting in chaotic reflections (Figure 5). The SCs with acoustically chaotic fill are less prevalent in seismic profiles, which are more frequently located near the middle part of the delta front. Collapses can trigger turbidity flows that rapidly accumulate various sediments, more likely forming chaotic reflection fills (Liu et al., 2023) (Figure 5). Rapid sediment deposition also prevents effective pore water expulsion, leaving the sediments weak and under-consolidated (Gao, 2011), destabilizing the strata, and significantly contributing to various submarine geological disasters.

5.3.3 Development of symmetric, asymmetric, and composite SCs

SGFs, similar to rivers, exhibit pronounced fluid properties primarily in the two-dimensional aspect (along the flow direction) but have weaker three-dimensional properties (laterally or in other directions) (Figure 5). Consequently, SCs and river channels have certain similarities in their morphological characteristics as well as in their formation. Our findings indicate that the timing of occurrence, transport paths, and the erosive impacts of SGFs along the delta front slope collectively contribute to the diverse cross-sectional features observed in SCs. A detailed analysis is provided in the following. It is worth noting that this discussion, based on different cross-sectional features of SCs, is not exhaustive and does not preclude other potential formations for these features (Figure 10).

Compared with river channel formations, symmetric SCs generally reflect the ideal conditions of incision driven by SGFs. This might occur when hyperpycnal flows transport downslope rapidly, eroding and incising the underlying strata (Zavala and Pan, 2018) (Figure 6). Alternatively, these flows may cause collapses and accumulations as they rapidly pass through steep slopes (Keopold, 1957) (Figure 6). Asymmetric SCs exhibit uneven incision rates or intensities on either side, where one side may erode steeply while the other does not erode or may even accumulate sediment. This condition might initiate lateral migration of the buried SCs (Liu et al., 2013; Huang et al., 2024) (Figure 6). An alternative explanation for asymmetric SCs is that submarine collapses or other sedimentary events along the path of hyperpycnal flows might change the direction of flows, causing enhanced erosion on one side and initiating lateral migration (Tek et al., 2021; Pope et al., 2022) (Figures 6, 10A). Additionally, the incision by SGFs can also trigger minor collapses of the internal side of the SCs, further promoting lateral migration (Mulder and Alexander, 2001; Bain and Hubbard, 2016; Huang et al., 2024) (Figures 6, 10B).

Composite SCs are most likely the result of multiple SGF events that travel along similar or overlapping paths on the slope (Figures 6, 10C). Due to the superposition of multiple SCs, this type can be quite large in scale (up to ca. 8 km), which is consistent with most of the observed composite SCs in the study area (Figure 6). As SGFs move downslope from higher elevations, the decreasing steepness of the terrain causes a reduction in flow energy closer to the source, leading to numerous SCs that frequently branch and merge, thereby promoting lateral migration (Sun et al., 2016). Additionally, collapses within these SCs may lead to the formation of new backward branches, ultimately creating

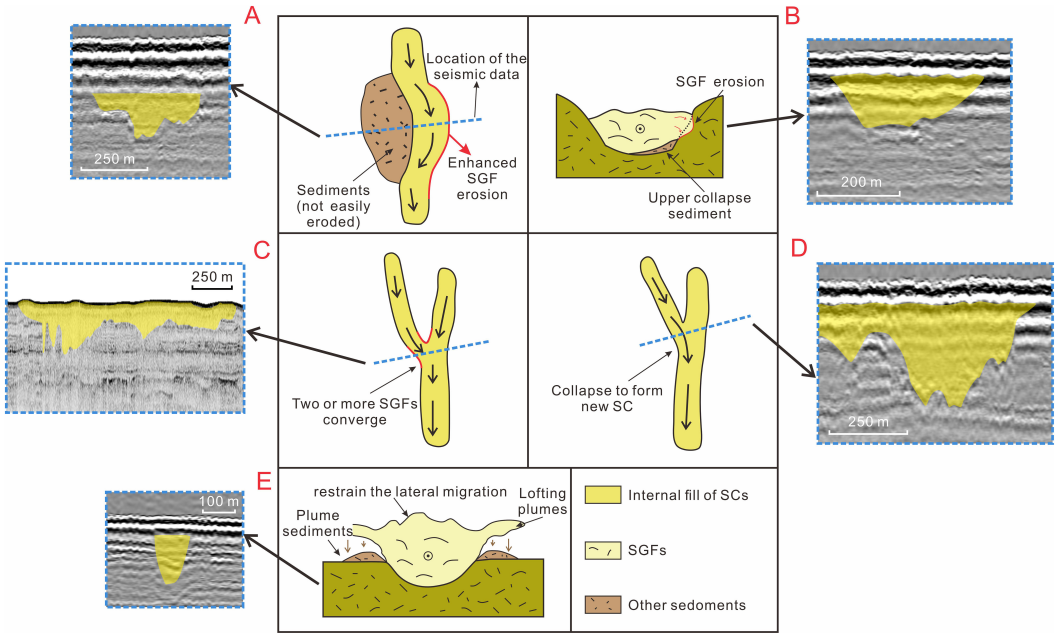

FIGURE 10
Schematic diagram depicting the development and representative seismic profiles of SCs with different cross-section morphology types, including asymmetric **(A, B)**, composite **(C, D)**, and symmetric **(E)** types (modified after Huang et al., 2024).

composite SCs (Pratson and Coakley, 1996) (Figures 6, 10D). Moreover, plumes from SGFs can elevate the sides of the SCs, enhancing confinement and thereby inhibiting lateral movement, which facilitates the formation of symmetric SCs (Labourdette and Bez, 2010; Hodgson et al., 2011) (Figure 10E).

5.4 The impact of lobe switching and longshore drifts on SC development

5.4.1 The impact of lobe switching event in 1976 CE

Between 1964 and 1976 CE, active sediment accumulation at the DKL resulted in the formation of high platforms as sediments continuously built up under the influence of the tidal shear front (Liu et al., 2022). The platforms facilitated the collapse- and resuspension-related SGFs and therefore the formation of SCs (e.g., Bornhold et al., 1986). Multiple episodes of SGFs, primarily hyperpycnal flows, initiated on the slope and moved downslope, eroding the seafloor and creating numerous SCs, which caused the widespread distribution of SCs on the delta front of DKL. As previously analyzed, these SCs are situated within Unit B, where hyperpycnal flow sediments are predominant (Figures 2, 9).

After 1976 CE, with the abandonment of the DKL and the activation of the QSGL, the DKL began to experience significant erosion, compounded by the erosion of the longshore transport and/or erosional regimes (Gao et al., 2018), which is evidenced by the truncation observed at the top of Unit B (Figure 2). Meanwhile, the under-consolidated sediments on the platforms became vulnerable to instability and collapse, leading to collapse-related SGFS, particularly the turbidity flows (Liu et al., 2022). These flows have since become the dominant type of SGFs in the area after the abandonment of the DKL, contributing to the formation of a new SGF Unit A, which has, in turn, generated additional SCs (SC1 in Figure 2). These younger SCs, located within Unit A, are differentiated from the lower SCs (SC2 in Figure 2) by erosional surfaces (R1) created by lobe switching (Figures 2, 9). In this regard, we exclude the possibility that these SCs are formed by high energy events such as storms.

5.4.2 The impact of longshore drifts on SC development

Sediments from the modern river mouth, flowing into the eastern part of the QSGL, have also created similar high platforms at the upper delta front (Liu et al., 2022). The SGF-related accumulations at the toe of the delta front, have therefore integrated with conventional deltaic accumulations formed by effluent sediments accumulation during the construction of the QSGL. These combined deposits are acoustically indistinguishable (Figure 7A). The numerous SCs identified there confirm the frequent occurrence of hyperpycnal flows, which dominate the formation of SGF-related accumulations, corroborating the observations by Wang (2012) in the eastern QSGL. Southeastern longshore drifts (driven by waves, tides, residual currents, and their combination) continue to impact these SGF units (Wiseman et al., 1986), leading to the lithology features of rework action (such as interbedded sand and mud layers and thin wavy sand/silt beds in Figure 7B) as well as further erosion and redistribution of these sediments. As mentioned earlier, the internal sediments of the SCs are due to rapid infilling by SGFs, combined with rapid overlying layers accumulation (especially at the east of the present-day active

QSGL). Therefore, it is unlikely that the longshore drifts rework will occur (Figures 1A, 7B).

In contrast, the area near the DKL lacks Unit A, and only one period of SC formation is evident (SC1 in Figure 2A). Unit A near the QSGL is thinner in the middle of the slope, and its R1 surface is truncated by the seafloor (Figure 2A), which are attributed to erosion from longshore drifts (Chen, 2009; Liu et al., 2022). The subaqueous delta near the DKL has undergone more extensive erosion compared to the QSGL (Chu et al., 2006). This erosion has resulted in the complete removal of all Unit A (including the SCs within it) near the DKL, as well as part of Unit B (Figure 2A). In contrast, the area near the QSGL has experienced less intense erosion, thus making the SCs of multiple periods at varying depths to be well preserved (Figures 2B, 9). It is expected that, for the foreseeable future, SCs driven by SGFs will continue to form along the delta front of the Huanghe subaqueous delta and affect its sedimentary evolution.

6 Conclusions

This study investigated the morphology, distribution, and development of submarine channels (SCs) in the modern Huanghe subaqueous delta using high-resolution seismic data, core samples, and historical bathymetric data.

(1) SCs are prevalent along the slope in the upper and middle parts of the delta front offshore of the modern Huanghe delta. They are typically located at or near the landward flanks of sediment gravity flow (SGF)-related accumulations. We identified two types of SCs: buried SCs, characterized by subsurface cut-and-fill structures and filled with acoustically transparent materials (mainly structureless muds) and chaotic reflections in places, formed by SGF incisions followed by rapid sediment accumulation; and exposed SCs, which occur when these incisions are not fully infilled by subsequent sedimentation and are marked by jagged or gullied seafloor features.

(2) SCs can be categorized based on cross-sectional morphology into symmetric, asymmetric, and composite types. They correspond to idealized SGF incision on the seafloor, uneven incision intensity on either side within the SCs, and the overlay of two or more symmetric or asymmetric SCs, respectively.

(3) The buried SCs at various depths correspond to distinct historical periods associated with the lobate evolution of the delta, specifically during 1855–1964 CE, 1964–1976 CE, and 1976–2007 CE. SCs near the Diaokou Lobe (DKL) are consistently found at a uniform depth beneath the seafloor, while those near the Qingshuigou Lobe (QSGL) are distributed at varying depths. The evolution of SGF-related deposits at the lower part of the delta front aligns with the formation of contemporaneous SCs at the middle and upper part of the delta front.

(4) Longshore drift significantly influences the geomorphological evolution of the delta front and SC development, particularly offshore from the DKL. This has resulted in extensive erosion of SCs off the DKL after 1976 CE, leaving only those formed during 1964–1976 CE preserved. In contrast, multi-stage SCs near the QSGL are well-preserved across different horizons.

Our findings highlight the complexity of spatial distribution and development of SC in the delta front and their close correlation with delta front evolution. This insight may contribute to understanding sedimentary and geomorphological processes in other shallow-water deltaic environments.

Data availability statement

The original contributions presented in the study are included in the article/supplementary material. Further inquiries can be directed to the corresponding author.

Author contributions

SA: Writing – original draft, Visualization, Methodology, Formal analysis, Data curation, Conceptualization. AF: Resources, Supervision, Writing – review & editing. WF: Formal analysis, Methodology, Writing – review & editing. YW: Writing – review & editing. YC: Formal analysis, Writing – review & editing. ZW: Writing – review & editing. XC: Writing – review & editing. YY: Investigation, Resources, Writing – review & editing. YP: Investigation, Resources, Writing – review & editing. SL: Conceptualization, Formal analysis, Resources, Supervision, Writing – review & editing.

Funding

The author(s) declare financial support was received for the research, authorship, and/or publication of this article. This work was sponsored by the National Natural Science Foundation of China (grants 42276175; 42076067), and the Shanghai Pilot Program for Basic Research (TQ20220101).

Acknowledgments

The authors would like to thank Ting Chen for providing access to the data from core YD02. Additionally, the authors acknowledge the assistance of ChatGPT, developed by OpenAI, in refining the English language usage in this manuscript, while not contributing to the creation of any new content.

Conflict of interest

Author YC was employed by POWERCHINA Huadong Engineering Corporation Limited.

The remaining authors declare that the research was conducted in the absence of any commercial or financial relationships that could be construed as a potential conflict of interest.

Publisher's note

References

Bain, H. A., and Hubbard, S. M. (2016). Stratigraphic evolution of a long-lived submarine channel system in the late cretaceous nanaimo group, British Columbia, Canada. *Sediment. Geol.* 337, 113–132. doi: 10.1016/j.marpetgeo.2024.106869

Bi, N., Wang, H., and Wu, X. (2021). Phase change in evolution of the modern Huanghe (Yellow River) Delta: Process, pattern, and mechanisms. *Mar. Geology.* 437, 106516. doi: 10.1016/j.margeo.2021.106516

Bi, N., Wang, H., and Yang, Z. (2014). Recent changes in the erosion–accretion patterns of the active Huanghe (Yellow River) delta lobe caused by human activities. *Continental Shelf Res.* 90, 70–78. doi: 10.1016/j.csr.2014.02.014

Bi, N., Yang, Z., and Wang, H. (2011). Seasonal variation of suspended-sediment transport through the southern Bohai Strait. *Estuarine. Coast. Shelf Science.* 93, 239–247. doi: 10.1016/j.ecss.2011.03.007

Bornhold, B. D., Yang, Z. S., and Keller, G. H. (1986). Sedimentary framework of the modern Huanghe (Yellow River) delta. *Geo-Marine Letters.* 6, 77–83. doi: 10.1007/BF02281643

Chang, F., and Jia, Y. (2010). Review of the studies on geo-hazards induced by liquefaction at the Yellow River subaqueous delta. *Mar. Geology Quaternary Geology.* 30, 145–151. doi: 10.3724/SP.J.1140.2010.05145

Chen, C. T. A. (2009). Chemical and physical fronts in the Bohai, Yellow and East China seas. *J. Mar. Systems.* 78, 394–410. doi: 10.1016/j.jmarsys.2008.11.016

Chen, T., Liu, Q., and Zheng, Y. (2021). Environmental magnetic properties of core sediments in the Yellow River subaqueous delta and their chronologicalapplications. *Chin. Sci. Bull.* 66 (30), 3902–3915. doi: 10.1360/TB-2021-0528

Chen, W., and Yang, Z. (1992). The classification and analysis of seafloor micromorphology on the Huanghe River (Yellow River) subaqueous slope. *J. Ocean Univ. Qingdao.* 01), 71–81. doi: 10.16441/j.cnki.hdxb.1992.01.009

Cheng, Y. J., and Cheng, J. G. (2000). Analysis of the current field in the new Yellow River entrance sea area. *Coast. Eng.* 19, 5–11.

Chu, Z. X., Sun, X. G., and Zhai, S. K. (2006). Changing pattern of accretion/erosion of the modern Yellow River (Huanghe) subaerial delta, China: Based on remote sensing images. *Mar. Geology* 227, 13–30. doi: 10.1016/j.margeo.2005.11.013

Coleman, J. M., Prior, D. B., and Garrison, L. E. (1980). *Subaqueous sediment instabilities in the offshore Mississippi River delta* (U.S: Department of the Interior, Bureau of Land Management Open-File Report).

Correggiar, A., Cattaneo, A., and Trincardi, F. (2005a). Depositional patterns in the late Holocene Po delta system. *geoscienceworld*, 365–392. doi: 10.2110/pec.05.83.0365

Correggiar, A., Cattaneo, A., and Trincardi, F. (2005b). The modern Po Delta system: lobe switching and asymmetric prodelta growth. *Mar. Geology* 222, 49–74. doi: 10.1016/j.margeo.2005.06.039

Daly, R. A. (1936). Origin of submarine canyons. *Am. J. Sci.* 5, 401–420.

Dasgupta, S., and Buatois, L. A. (2015). High-frequency stacking pattern and stages of canyon/gully evolution across a forced regressive shelf-edge delta-front. *Mar. Petroleum Geology* 68, 40–53. doi: 10.1016/j.marpetgeo.2015.08.003

Fan, H., Huang, H., and Zeng, T. (2006). Impacts of anthropogenic activity on the recent evolution of the Huanghe (Yellow) River Delta. *J. Coast. Res.* 22, 919–929. doi: 10.2112/04-0150.1

Fan, D., Wang, Y., and Liu, M. (2013). Classifications, sedimentary features and facies associations of tidal flats. *J. Palaeogeogr.* 2, 66–80. doi: 10.3724/SP.J.1261.2013.00018

Feng, W., Liu, S., and Li, W. (2024). Seismic investigation uncovers formation and spatial distribution of seafloor erosional features on the Changjiang (Yangtze) River subaqueous delta. *Mar. Geology* 470, 107268. doi: 10.1016/j.margeo.2024.107268

Feng, X., Qi, H., Wang, T., Li, A., and Lin, L. (2004). Geomorphological evolution and geological disasters analysis in Chengdao sea area of the Yellow River Delta. *Rock Soil mechanics* 25, 17–20. doi: 10.16285/j.rsm.2004.s1.004

Fu, Y., Chen, S., Ji, H., Fan, Y., and Li, P. (2021). The modern Yellow River Delta in transition: Causes and implications. *Mar. Geology* 436, 106476. doi: 10.1016/j.margeo.2021.106476

Gao, W. (2011). Stratigraphy sequence of diaokou lobe in the modern yellow river delta. [Phd thesis]. Qingdao, China: Ocean University of China.

Gao, W., Liu, S., Liu, J., Xu, Y., and Li, P. (2018). The sedimentary facies and dynamic environment of the Diaokou lobe in the modern Huanghe River Delta of China. *Acta Oceanologica Sinica.* 37, 40–52. doi: 10.1007/s13131-018-1332-z

Hodgson, D. M., Di Celma, C. N., Brunt, R. L., and Flint, S. S. (2011). Submarine slope degradation and aggradation and the stratigraphic evolution of channel–levee systems. *J. Geological Soc.* 168, 625–628. doi: 10.1144/0016-76492010-177

Hu, W., Liu, S., Liu, Y., Feng, A., Feng, W., and Wang, X. (2024). Pollen and spore records constrained by millennial prodelta evolution: a case study of the Huanghe (Yellow River) delta. *Front. Mar. Sci.* 11. doi: 10.3389/fmars.2024.1378724

Huang, K., Zhong, G., He, M., Zhu, W., and Wu, Z. (2024). Migration and controls of Shenhu submarine canyons in the upper continental slope of northern South China Sea: Insights from three-dimensional seismic data mapping. *Sedimentology*. 71, 2009–2034. doi: 10.1111/sed.13201

Jeng, D. S. (2001). Mechanism of the wave-induced seabed instability in the vicinity of a breakwater: a review. *Ocean Eng.* 28, 537–570. doi: 10.1016/S0029-8018(00)00013-5

Jiang, C., Chen, S., Pan, S., Fan, Y., and Ji, H. (2018). Geomorphic evolution of the Yellow River Delta: Quantification of basin-scale natural and anthropogenic impacts. *Catena* 163, 361–377. doi: 10.1016/j.catena.2017.12.041

Keopold, L. B. (1957). River channel patterns: braided, meandering and straight US Geol. *Survey Prof. Paper* 282, 39–84. doi: 10.3133/pp282B

Labourdette, R., and Bez, M. (2010). Element migration in turbidite systems: Random or systematic depositional processes. *AAPG Bull.* 94, 345–368. doi: 10.1306/09010909035

Lamb, M. P., and Mohrig, D. (2009). Do hyperpycnal-flow deposits record river-flood dynamics? *Geology* 37, 1067–1070. doi: 10.1130/G30286A.1

Li, P. (2015). Formation mechanism and division of typical geological hazards on the surface and shall of the yellow river delta offshore [Phd thesis]. Ocean University of China.

Li, G., Cheng, G., Wei, H., Pan, W., Ren, Y., Ding, D., et al. (1994). Shear front in the modern Yellow River mouth. *Chin. Sci. Bull.* 10), 928–932. doi: 10.1360/csb1994-39-10-928

Li, G., Tang, Z., Yue, S., Zhuang, K., and Wei, H. (2001). Sedimentation in the shear front of the Yellow River mouth. *Continental Shelf Res.* 21, 607–625. doi: 10.1016/S0278-4343(00)00097-2

Li, G., Zhuang, K., and Jiang, Y. (2000). Engineering instability of the deposition bodies in the yellow river delta. *Mar. Geology &Quaternary Geology.* 02), 21–26. doi: 10.16562/j.cnki.0256-1492.2000.02.004

Liu, S., Feng, A., Du, J., Xia, D., Li, P., Xue, X., et al. (2014). Evolution of the buried channel systems under the modern Yellow River Delta since the Last Glacial Maximum. *Quaternary Int.* 349, 327–338. doi: 10.1016/j.quaint.2014.06.061

Liu, S., Feng, A., Li, P., Du, J., and Hu, W. (2013). Preliminary analysis of the ancient channels buried shallower than 50 meters in the coastal and offshore areas of the yellow river delta. *Coast. Eng. J.* 32, 22–30. doi: 10.3969/j.issn.1002-3682.2013.04.004

Liu, S., Feng, A., Liu, C., Zheng, Y., Li, P., and Zhang, Z. (2019). Seismic stratigraphy and morphology of the Holocene progradational system beneath Bohai Bay, Bohai Sea: Lobate evolution of a multi-sourced subaqueous fluviodeltaic complex. *Mar. Geology* 409, 31–47. doi: 10.1016/j.margeo.2018.12.009

Liu, S., Goff, J. A., Gao, S., Feng, A., Wang, Y., Jia, J., et al. (2022). The impact of gravity-driven sedimentation on reshaping the huanghe (Yellow river) delta front. *J. Geophysical Research: Earth Surface* 127, e2022JF006717. doi: 10.1029/2022JF006717

Liu, S., Li, P., Feng, A., Du, J., Gao, W., Xu, Y., et al. (2016). Seismic and core investigation on the modern Yellow River Delta reveals the development of the uppermost fluvial deposits and the subsequent transgression system since the postglacial period. *J. Asian Earth Sci.* 128, 158–180. doi: 10.1016/j.jseaes.2016.07.009

Liu, M., Wang, Z., Yu, K., and Xu, J. (2023). Two distinct types of turbidity currents observed in the Manila Trench, South China Sea. *Commun. Earth Environ.* 4, 108. doi: 10.1038/s43247-023-00776-8

Liu, F. (1985). The characteristics of main stream of Yellow River flowing into the sea changing with tidal current and the moving directions of silt. *Trans. Oceanology Limnology* 2, 20–23. doi: 10.13984/j.cnki.cn37-1141.1985.02.006

Luan, G., Dong, C., Lin, C., Ren, L., Jiao, H., Zhao, H., et al. (2018). Development conditions, evolution process and depositional features of hyperpycnal flow. *Oil& Gas Geology.* 39, 438–453. doi: 10.11743/ogg20180303

Luo, D., and Liu, H. (2015). Numerical study on the tides and tidal currents in the Bohai Sea. *J. Shanghai Ocean University.* 24, 457–464.

Malonely, J. M., Bentley, S. J., Xu, K., Obelcz, J., Georgiou, L., Jafari, N., et al. (2020). Mass wasting on the Mississippi River subaqueous delta. *Earth-Science Rev.* 200, 103001. doi: 10.1016/j.earscirev.2019.103001

Masson, D. G., Harbitz, C. B., Wynn, R. B., Pedersen, G., and Løvholt, F. (2006). Submarine landslides: processes, triggers and hazard prediction. *Philos. Trans. R. Soc. A: Mathematical Phys. Eng. Sci.* 364, 2009–2039. doi: 10.1098/rsta.2006.1810

Mulder, T., and Alexander, J. (2001). The physical character of subaqueous sedimentary density flows and their deposits. *Sedimentology* 48, 269–299. doi: 10.1046/j.1365-3091.2001.00360.x

Mulder, T., Syvitski, J. P. M., Migeon, S., Faugeres, J., and Savoye, B. (2003). Marine hyperpycnal flows: initiation, behavior and related deposits. *A review. Mar. Petroleum Geology* 20, 861–882. doi: 10.1016/j.marpetgeo.2003.01.003

Pang, J. (1979). Evolution of the Yellow River mouth: I. Historical shifts. *Oceonologia Limnologia Sinica.* 10, 136.

Pang, J., and Si, S. (1980). Fluvial process of the Huanghe River Estuary II-Hydrographical character and the region of sediment silting. *Oceanologia Limnologia Sinica.* 11, 295–305.

Peng, J., Chen, S., Chen, Y., and Li, G. (2014). Geological hazards and their spatial distribution in the subaqueous slope at the erosive coast of the Yellow River delta. *Mar. Sci. Bulletin.* 33, 1–6. doi: 10.11840/j.issn.1001-6392.2014.01.001

Pope, E. L., Heijnen, M. S., Talling, P. J., Jacinto, R. S., Gaillot, A., Baker, M., et al. (2022). Carbon and sediment fluxes inhibited in the submarine Congo Canyon by landslide-damming. *Nat. Geoscience.* 15, 845–853. doi: 10.1038/s41561-022-01017-x

Prasojo, O. A., Hoey, T. B., Owen, A., and Williams., R. (2024). Influence of alluvial slope on avulsion in river deltas. *EGUsphere*, 1-24. doi: 10.5194/egusphere-2024-2113

Pratson, L. F., and Coakley, B. J. (1996). A model for the headward erosion of submarine canyons induced by downslope-eroding sediment flows. *Geological Soc. America Bulletin.* 108, 225–234. doi: 10.1130/0016-7606(1996)108<0225:AMFTHE>2.3.CO;2

Prior, D. B., Yang, Z.-S., Bornhold, B. D., Keller, G. H., Lin, Z. H., Wiseman, W. J., et al. (1986). The subaqueous delta of the modern Huanghe (Yellow River). *Geo-Marine Lett.* 6, 67–75. doi: 10.1007/BF02281642

Ren, Z., Zhan, C., Yu, J., Geng, W., Cao, Y., and Wang, Q. (2022). Analysis of coastline changes in the abandoned sub-delta of Diaokou over the past 50 years. *Mar. Sci.* 46, 8–19. doi: 10.11759/hykx20220327001

Roberts, H. H., Suhayda, J. N., and Coleman, J. M. (2020). "Sediment deformation and transport on low-angle slopes: Mississippi River delta," in *Thresholds in geomorphology* (Routledge), 131–167. doi: 10.4324/9781003028697-7

Sun, F., Yang, R., and Li, D. (2016). Research progresses on hyperpycnal flow deposits. *Acta Sedimentologica Sin.* 34, 452–462. doi: 10.14027/j.cnki.cjxb.2016.03.003

Tang, M. (2020). Turbidity Process and Sedimentary Environment of South East Canada (Atlantic) Continental Slope – Case study of Halibut Canyon. [Phd thesis]. Nanjing, China: School of Geography and Ocean Science, Nanjing University Key Laboratory of Coast and Island Development of the Ministry of Education.

Tek, D. E., Mcaryhur, A. D., Poyatos-more, M., Colombera, L., Patacci, M., Craven, B., et al. (2021). Relating seafloor geomorphology to subsurface architecture: How mass-transport deposits and knickpoint-zones build the stratigraphy of the deep-water Hikurangi Channel. *Sedimentology.* 68, 3141–3190. doi: 10.1111/sed.12890

Vanneste, M., Sultan, N., Garziglia, S., Forsberg, C., and L'Heureux, J. (2014). Seafloor instabilities and sediment deformation processes: The need for integrated, multi-disciplinary investigations. *Mar. Geology* 352, 183–214. doi: 10.1016/j.margeo.2014.01.005

Wang, F., and Su, Z. (1989). The distribution characteristic of tidal currents off coast of the Yellow River estuary gate. *Trans. Oceanology Limnology. Trans. Oceanology Limnology* 2), 8–11. doi: 10.13984/j.cnki.cn37-1141.1989.02.002

Wang, A., and Ye, Y. (1990). Framework, Developing processes and sedimentary model of the modern Huanghe River delta. *Mar. Geology& Quaternary Geology* 10, 1–12. doi: 10.16562/j.cnki.0256-1492.1990.01.001

Wang, Y. (2012). Process of high-concentrated sediment hyperpycnal flow at the Huanghe River Mouth: *in-situ* observations and numerical simulation. [Phd thesis]. Ocean University of China.

Wang, H., and Liu, H. (2016). Evaluation of storm wave-induced silty seabed instability and geo-hazards: A case study in the Yellow River delta. *Appl. Ocean Res.* 58, 135–145. doi: 10.1016/j.apor.2016.03.013

Wang, Z., Sun, Y., Jia, Y., Shan, Z., Shan, H., Zhang, S., et al. (2020). Wave-induced seafloor instabilities in the subaqueous Yellow River Delta—initiation and process of sediment failure. *Landslides* 17, 1849–1862. doi: 10.1007/s10346-020-01399-2

Wang, H., Wang, A., Bi, N., Zeng, X., and Xiao, H. (2014). Seasonal distribution of suspended sediment in the Bohai Sea, China. *Continental Shelf Res.* 90, 17–32. doi: 10.1016/j.csr.2014.03.006

Wang, H., Yang, Z., Li, Y., Guo, Z., Sun, X., and Wang, Y. (2007). Dispersal pattern of suspended sediment in the shear frontal zone off the Huanghe (Yellow River) mouth. *Continental Shelf Res.* 27, 854–871. doi: 10.1016/j.csr.2006.12.002

Wen, M., Wang, Z., Zhang, B., Zhang, S., and Jia, Y. (2018). Survey on the distribution of fluid mud and disturbed strata on subaqueous Yellow River delta. *J. Eng. Geology.* 26, 677–683. doi: 10.13544/j.cnki.jeg.2018225

Wiseman, W. J., Fan, Y. B., Bornhold, B. D., Keller, G. H., Su, Z., Prior., D. B., et al. (1986). Suspended sediment advection by tidal currents off the Huanghe (Yellow River) delta. *Geo-Marine Letters.* 6, 107–113. doi: 10.1007/BF02281646

Wright, L. D., Yang, Z. S., Bornhold, B. D., Keller, G. H., Prior., D. B., and Wiseman, W. J. (1986). Hyperpycnal plumes and plume fronts over the Huanghe (Yellow River) delta front. *Geo-Marine Letters.* 6, 97–105. doi: 10.1007/BF02281645

Wrihjt, L. D., Wiseman, W. J., Bornhold, B. D., Prior., D. B., Suhayda, J. N., Keller, G. H., et al. (1988). Marine dispersal and deposition of Yellow River silts by gravity-driven underflows. *Nature.* 332, 629–632. doi: 10.1038/332629a0

Wu, X., Bi, N., Xu, J., Nittrouer, J. A., Yang, Z., Saito, Y., et al. (2017). Stepwise morphological evolution of the active Yellow River (Huanghe) delta lobe, (1976-2013): Dominant roles of riverine discharge and sediment grain size. *Geomorphology* 292, 115–127. doi: 10.1016/j.geomorph.2017.04.042

Xiong, X. (2012). *Chinese offshore oceanography - physical oceanography and marine meteorology* (Beijing: Ocean Press).

Xu, J. (2014). Turbidity current research in the past century: an overview. *Periodical Of Ocean Univ. China.* 44, 98–105. doi: 10.16441/j.cnki.hdxb.2014.10.014

Xu, G., Sun, Y., Wang., X., Hu, G., and Song, Y. (2009). Wave-induced shallow slides and their features on the subaqueous Yellow River delta. *Can. Geotechnical J.* 46, 1406–1417. doi: 10.1139/T09-068

Xu, G., Wei, C., Sun, Y., and Song, Y. (2008). The engineering characteristics of shallow disturbed strata and analysis of their formation on the subaqueous Yellow River Delta. *Mar. Geology Quaternary Geology.* 28, 19–25. doi: 10.3724/SP.J.1140.2008.06019

Xue, C. (1994). Division and recognition of modern Yellow River delta lobes. *Geographical Res.* 13, 59–66.

Xue, C. (2009). Historical changes of coastlines on west and south coasts of Bohai Sea since 7000 a BP. *Scientia Geographica Sinica.* 29, 217–222. doi: 10.13249/j.cnki.sgs.2009.02.217

Xue, C., Ye, S., Gao, M., and Ding, X. (2009). Determination of depositional age in the Huanghe Delta in China. *Acta oceanological Sinica.* 31, 117–124. doi: 10.3321/j.issn:0253-4193.2009.01.015

Yang, Z., Chen, W., Chen, Z., Wu, G., Cao, L., and Shen, W. (1994). Subaqueous landslide system in the Huanghe River (Yellow River) delta. *Oceanologia Limnologia Sinica.* 25 (6), 573–581. doi: 10.3321/j.issn:0029-814X.1994.06.001

Yang, Z., Li, G., Wang, H., Hu, B., and Cheng, Y. (2008). Variation of daily water and sediment discharge in the Yellow River lower reaches in the past 55years and its response to the dam operation on its main stream. *Mar. Geology& Quaternary Geology.* 28, 9–18. doi: 10.3724/SP.J.1140.2008.06009

Yang, H., Yang, S., Xu, K., Wu, H., Shi, B., Zhu, Q., et al. (2017). Erosion potential of the Yangtze Delta under sediment starvation and climate change. *Sci. Rep.* 7, 10535. doi: 10.1038/s41598-017-10958-y

Ye, Z., Yang, N., Cui, L., and Ma, X. (2023). Analysis of tidal curent characteristics in the sea near the Yelow River Mouth. *Trans. Oceanology Limnology* 45, 94–100. doi: 10.13984/j.cnki.cn37-1141.2023.02.012

Yu, H., Liu, X., Lu, Y., Li, W., Gao, H., Wu, R., et al. (2022). Characteristics of the sediment gravity flow triggered by wave-induced liquefaction on a sloping silty seabed: an experimental investigation. *Front. Earth Sci.* 10. doi: 10.3389/feart.2022.909605

Yu, Y., Wang, H., Shi, X., Ran, X., Cui, T., Qiao, S., et al. (2013). New discharge regime of the Huanghe (Yellow River): Causes and implications. *Continental Shelf Res.* 69, 62–72. doi: 10.1016/j.csr.2013.09.013

Zavala, C. (2020). Hyperpycnal (over density) flows and deposits. *J. Palaeogeogr.* 9, 17. doi: 10.1186/s42501-020-00065-x

Zavala, C., Arcuri, M., Gamero, H., Contreras, C., and Meglio, D. M. (2011). A genetic facies tract for the analysis of sustained hyperpycnal flow deposits. *Geology* 61, p. 31–51. doi: 10.1306/13271349St613438

Zavala, C., and Pan, S. X. (2018). Hyperpycnal flows and hyperpycnites: Origin and distinctive characteristics. *Lithologic Reservoirs.* 30, 1–27. doi: 10.3969/j.issn.1673-8926.2018.01.001

Zavala, C., Valiente, L. B., and Vallez, Y. (2006). Ancient Lacustrine hyper pycnites: a depositionalmodel from a case study in the Rayoso Formation (Cretaceous) of west -central Argentina. Journal of Sedimentary Research 76. 40–58. doi: 10.2110/jsr.2006.12

Zhang, J., Yang, Z., and Shi, M. (1998). *Suspended sediment regime in the Huanghe River Estuary and South Bohai Sea, II. Observations in the South Bohai Sea. Land–sea interaction in Chinese Coastal Zones* (Being: China Ocean Press), 44–57.

Zhao, B., Zhuang, G., Cao, D., and Lei, F. (1995). Circulation, tidal residual currents and their effects on the sedimentations in the Bohai Sea. *Oceanologia Limnologia Sinica.* 05), 466–473.

Zhou, L., Liu, J., Saito, Y., Gao, M., Diao, S., Qiu, J., et al. (2016). Modern sediment characteristics and accumulation rates from the delta front to prodelta of the Yellow River (Huanghe). *Geo-Mar Lett.* 36, 247–258. doi: 10.1007/s00367-016-0442-x